The Astrophysical Journal, 734:31 (11pp), 2011 June 10 doi:10.1088/0004-637X/734/1/31


# THE FAR-ULTRAVIOLET "CONTINUUM" IN PROTOPLANETARY DISK SYSTEMS. II. CARBON MONOXIDE FOURTH POSITIVE EMISSION AND ABSORPTION*

Kevin France[1], Eric Schindhelm[1], Eric B. Burgh[1], Gregory J. Herczeg[2], Graham M. Harper[3], Alexander Brown[1], James C. Green[1], Jeffrey L. Linsky[4], Hao Yang[4], Hervé Abgrall[5], David R. Ardila[6], Edwin Bergin[7], Thomas Bethell[7], Joanna M. Brown[2], Nuria Calvet[7], Catherine Espaillat[8,14], Scott G. Gregory[9], Lynne A. Hillenbrand[9], Gaitee Hussain[10], Laura Ingleby[7], Christopher M. Johns-Krull[11], Evelyne Roueff[5], Jeff A. Valenti[12], and Frederick M. Walter[13]

[1] Center for Astrophysics and Space Astronomy, University of Colorado, 389 UCB, Boulder, CO 80309, USA; kevin.france@colorado.edu
[2] Max-Planck-Institut für Extraterrestriche Physik, Postfach 1312, 85741 Garching, Germany
[3] School of Physics, Trinity College, Dublin 2, Ireland
[4] JILA, University of Colorado and NIST, 440 UCB, Boulder, CO 80309, USA
[5] LUTH and UMR 8102 du CNRS, Observatoire de Paris, Section de Meudon, Place J. Janssen, 92195 Meudon, France
[6] NASA Herschel Science Center, California Institute of Technology, 1200 East California Boulevard, Pasadena, CA 91125, USA
[7] Department of Astronomy, University of Michigan, 830 Dennison Building, 500 Church Street, Ann Arbor, MI 48109, USA
[8] Harvard-Smithsonian Center for Astrophysics, 60 Garden Street, MS-78, Cambridge, MA 02138, USA
[9] California Institute of Technology, Department of Astrophysics, MC 249-17, Pasadena, CA 91125, USA
[10] ESO, Karl-Schwarzschild-Strasse 2, 85748 Garching bei München, Germany
[11] Department of Physics & Astronomy, Rice University, Houston, TX 77005, USA
[12] Space Telescope Science Institute, 3700 San Martin Drive, Baltimore, MD 21218, USA
[13] Department of Physics and Astronomy, Stony Brook University, Stony Brook, NY 11794-3800, USA
*Received 2011 January 17; accepted 2011 April 3; published 2011 May 23*

## ABSTRACT

We exploit the high sensitivity and moderate spectral resolution of the *Hubble Space Telescope* Cosmic Origins Spectrograph to detect far-ultraviolet (UV) spectral features of carbon monoxide (CO) present in the inner regions of protoplanetary disks for the first time. We present spectra of the classical T Tauri stars HN Tau, RECX-11, and V4046 Sgr, representative of a range of CO radiative processes. HN Tau shows CO bands in absorption against the accretion continuum. The CO absorption most likely arises in warm inner disk gas. We measure a CO column density and rotational excitation temperature of $N(\mathrm{CO}) = (2 \pm 1) \times 10^{17}$ cm$^{-2}$ and $T_{\mathrm{rot}}(\mathrm{CO})$ 500 $\pm$ 200 K for the absorbing gas. We also detect CO $A$–$X$ band emission in RECX-11 and V4046 Sgr, excited by UV line photons, predominantly H I Ly$\alpha$. All three objects show emission from CO bands at $\lambda > 1560$ Å, which may be excited by a combination of UV photons and collisions with non-thermal electrons. In previous observations these emission processes were not accounted for due to blending with emission from the accretion shock, collisionally excited $H_2$, and photo-excited $H_2$, all of which appeared as a "continuum" whose components could not be separated. The CO emission spectrum is strongly dependent upon the shape of the incident stellar Ly$\alpha$ emission profile. We find CO parameters in the range: $N(\mathrm{CO}) \sim 10^{18}$–$10^{19}$ cm$^{-2}$, $T_{\mathrm{rot}}(\mathrm{CO}) \gtrsim 300$ K for the Ly$\alpha$-pumped emission. We combine these results with recent work on photo-excited and collisionally excited $H_2$ emission, concluding that the observations of UV-emitting CO and $H_2$ are consistent with a common spatial origin. We suggest that the CO/$H_2$ ratio ($\equiv N(\mathrm{CO})/N(\mathrm{H_2})$) in the inner disk is $\sim$1, a transition between the much lower interstellar value and the higher value observed in solar system comets today, a result that will require future observational and theoretical study to confirm.

*Key words:* protoplanetary disks – stars: individual (HN Tau, RECX-11, V4046 Sgr)

*Online-only material:* color figures

## 1. INTRODUCTION

Observations of classical T Tauri star (CTTS) disks offer a snapshot of the formation epoch of Jovian extrasolar planets. While the majority of the mass in these young disks (age $\lesssim$ 10 Myr) is in the form of molecular hydrogen ($H_2$), the lack of a permanent dipole moment makes $H_2$ gas difficult to observe in the cool outer regions of the protoplanetary disk. Millimeter and submillimeter observations of CO can be used to trace molecular material in the outer disk (e.g., Dutrey et al. 1996; Qi et al. 2004), while near- and mid-infrared (IR) observations of OH, CO, $CO_2$, $H_2O$, and other molecules are powerful diagnostics of inner gas disks ($a < 5$ AU), the region of terrestrial planet formation (Najita et al. 2003; Carr et al. 2004; Salyk et al. 2007, 2008; Carr & Najita 2008; Bethell & Bergin 2009). IR observations of the overtone ($\Delta v = 2$) and fundamental ($\Delta v = 1$) bands of CO have been the most widely used tracers of the inner gas disk. The overtone bands are thought to trace the atmosphere of the optically thick gas at the very inner regions of the disk ($a \lesssim 0.2$ AU), where the temperature and densities are high ($T \approx$ 2000–3000 K, $n_H > 10^{10}$ cm$^{-3}$; Najita et al. 1996; Carr et al. 2004). The fundamental CO emission spectrum traces gas at $T \approx$ 1000–2000 K and radii $0.04 < a \lesssim 1$ AU (Najita et al. 2003, 2007), possibly arising in a disk atmosphere or regions of lower column density cleared out by dynamical processes (e.g., binary stellar systems or planetary interactions).

Far-ultraviolet (UV) observations of CTTSs reveal a wealth of emission lines arising from $H_2$, whose electronic transition spectrum is dipole-allowed. Far-UV $H_2$ was first identified in

* Based on observations made with the NASA/ESA *Hubble Space Telescope*, obtained from the data archive at the Space Telescope Science Institute. STScI is operated by the Association of Universities for Research in Astronomy, Inc., under NASA contract NAS 5-26555.
[14] NSF Astronomy and Astrophysics Postdoctoral Fellow.

CTTSs by Brown et al. (1981), and subsequent observations at higher spectral resolution (Herczeg et al. 2002; Ardila et al. 2002; Herczeg et al. 2006) have shown that this emission arises in a photo-excited ("pumped") warm surface layer of the disk (Herczeg et al. 2004) or in extended outflows (Walter et al. 2003; Saucedo et al. 2003). Recent observations have confirmed this picture, detecting both the fluorescent emission lines of $H_2$ and the absorption of pumping photons from the disk-reflected Ly$\alpha$ profile (Yang et al. 2011). Collisional excitation of $H_2$ by non-thermal electrons has been proposed to explain the faint 1300–1650 Å emission in CTTS disks (Bergin et al. 2004). Subsequent work has shown this excess to be ubiquitous (Ingleby et al. 2009), but the low spectral resolution and high detector backgrounds of the *Hubble Space Telescope* (*HST*) Advanced Camera for Surveys and Space Telescope Imaging Spectrograph, respectively, could not cleanly separate the components of this far-UV "continuum." France et al. (2011, hereafter Paper I) used the dramatic gains in spectroscopic sensitivity offered by *HST* Cosmic Origins Spectrograph (COS) to separate and identify three components of the faint excess emission. We use the term "continuum" because these emissions were mostly unresolved in previous studies. The purpose of this series of papers is to distinguish continuum and line-emission processes in CTTS spectra, and use this information to better understand two regions where far-UV photons are emitted: the accretion shock and the inner molecular disk. Paper I describes the accretion continuum and electron-excited $H_2$ spectrum for two prototypical objects. In the present work, we present the first detections of emission and absorption from the CO Fourth Positive band system ($A^1\Pi$–$X^1\Sigma^+$) in protoplanetary disks. These bands are observed in the wavelength range 1270 Å $\lesssim \lambda \lesssim$ 1720 Å.

While emission and absorption from the Fourth Positive band system are widely used molecular tracers in other areas of astrophysics, this is the first instance to our knowledge where these lines have been seen in young, low-mass protoplanetary disks. We provide this very brief review of $A$–$X$ observations in other astrophysical environments because the literature in these fields is considerably more developed than what exists for protoplanetary disks. The absorption bands of CO have been long studied in the interstellar medium (ISM) (Federman et al. 1980; Morton & Noreau 1994; Burgh et al. 2007; Sheffer et al. 2008). Absorption lines from cold CO have been seen in older debris disks (e.g., $\beta$ Pic, age $\sim$ 8–20 Myr; Vidal-Madjar et al. 1994; Roberge et al. 2000) and in the disk of the Herbig Ae star AB Aur (age $\approx$ 2 Myr; Roberge et al. 2001). In these cases, the CO is too cold to be in the inner disk, and may be replenished by the collision of planetesimals. The $A$–$X$ emission bands of CO are prominent in the far-UV spectra of comets (Feldman & Brune 1976; McPhate et al. 1999; Lupu et al. 2007), Venus (Durrance 1981; Hubert et al. 2010), and Mars (Feldman et al. 2000; Krasnopolsky & Feldman 2002). Emission and absorption spectra of CO have been observed in the atmospheres of cool stars (Carpenter et al. 1994; Hinkle et al. 2005), including the Sun (Goldberg et al. 1965; Bartoe et al. 1978), and dominate the far-UV spectrum of the Red Rectangle (HD 44179; see Sitko et al. 2008, and references therein). In this work we describe how the far-UV emission and absorption bands of CO can be used to constrain the molecular properties of protoplanetary disks.

We use three objects as prototypical examples of the range of CO spectral signatures in these objects. The spectra can be categorized as CO emission dominated by strong Ly$\alpha$ pumping (V4046 Sgr), CO emission coming from a combination of Ly$\alpha$ and C IV pumping photons with a possible contribution from electron-impact excitation (RECX-11), and CO absorption through a disk (HN Tau). In Section 2, we describe the targets and COS observations. In Section 3, we describe the qualitative features of the CO spectrum and present simple models for the emission and absorption. We use these results to constrain the physical conditions of the inner molecular disk and the CO/$H_2$ ratio in Section 4. We present a brief summary of the paper in Section 5.

## 2. TARGETS AND OBSERVATIONS

HN Tau, RECX-11, and V4046 Sgr are pre-main-sequence systems with actively accreting disks. These targets are found in associations typical of "young" (HN Tau) and "old" (RECX-11 and V4046 Sgr) disk populations. HN Tau is a 3.″1 ($\approx$430 AU) separation binary consisting of a K5 primary and mid-M secondary with masses of 0.8 and 0.2 $M_\odot$ (White & Ghez 2001). HN Tau A was the only stellar component in the spectroscopic aperture used in this work. This system is a member of the well-studied Taurus star-forming complex at a distance of $d \sim 140$ pc. HN Tau has strong outflows that have been studied extensively with optical spectroscopy (Hartigan et al. 2004). The typical age for young, gas- and dust-rich disks in the Taurus region is $\sim$1–2 Myr (Kenyon & Hartmann 1995). This is roughly consistent with the work of Kraus & Hillenbrand (2009), who find ages of $\approx$2 and 4 Myr for HN Tau A and B, respectively. HN Tau is heavily veiled in the optical, and observations of the outer dust disk at 850 $\mu$m indicate a dust mass of $\approx$270 $M_\oplus$ (Andrews & Williams 2005). The inclination of HN Tau is not known.

RECX-11 is a K5.5 candidate CTTS (Luhman & Steeghs 2004) with a mass of 0.9 $M_\odot$ (Mamajek et al. 1999). The disk inclination is estimated to be $i \approx 70^\circ$ based on magnetospheric accretion model fits to the H$\alpha$ line profile observed by Lawson et al. (2004). It is a member of the $\eta$ Cha star cluster, located at a distance of 97 pc (Mamajek et al. 1999). The cluster is estimated to have an age of 5–8 Myr (Mamajek et al. 1999; Luhman & Steeghs 2004), suggesting that the disk systems in $\eta$ Cha are likely to be in the process of dissipating their primordial gas envelopes; however RECX-11 displays a near-IR excess that is consistent with gas-rich, dusty CTTS disks in the younger Taurus cluster (Sicilia-Aguilar et al. 2009). The H$\alpha$ profile of RECX-11 suggests that it could be an accreting system (Jayawardhana et al. 2006), and as we will show in Section 3.2, this object displays far-UV continuum emission characteristic of weak accretion. Similarly, Ingleby et al. (2011) use a combination of far- and near-UV spectra to infer active accretion onto RECX-11, confirming its status as a CTTS. RECX-11 was part of a near-IR survey to measure the $H_2$ content of the inner disk, but no warm ($T \sim 2000$ K) $H_2$ was detected (Ramsay Howat & Greaves 2007). The non-detection of the near-IR rovibrational emission of $H_2$, contrasted with the $\sim$100 photo-excited $H_2$ emission lines observed in the COS data (Ingleby et al. 2011; this work), is a powerful demonstration of the utility of far-UV molecular observations in the study of the inner regions of protoplanetary disks.

V4046 Sgr is a close binary ($r \approx 9\,R_\odot$) composed of two mid-K stars (0.91 and 0.87 $M_\odot$; Stempels & Gahm 2004) with a circumbinary disk at an intermediate inclination angle (binary system and disk inclinations of $i \sim 35^\circ$; Quast et al. 2000; Rodriguez et al. 2010). It is one of the brightest CTTSs in the UV and X-ray bands (Günther et al. 2006; Günther & Schmitt 2008), located at a distance of 72 pc (Torres et al. 2006). It has an

**Table 1**
*HST*-COS Observing Log

| Object | R.A. (J2000) | Decl. (J2000) | Date | COS Modes | $T_{exp}$[G130M] (s) | $T_{exp}$[G160M] (s) |
|---|---|---|---|---|---|---|
| RECX-11 | $08^h47^m01\overset{s}{.}28$ | $-78°59'34\overset{''}{.}1$ | 2009 Dec 12 | G130M, G160M | 3645 | 4514 |
| HN Tau | $04^h33^m39\overset{s}{.}37$ | $+17°51'52\overset{''}{.}1$ | 2010 Feb 10 | G130M, G160M | 5725 | 4529 |
| V4046 Sgr | $18^h14^m10\overset{s}{.}49$ | $-32°47'34\overset{''}{.}2$ | 2010 Apr 27 | G130M, G160M | 4504 | 5581 |

age between 4 and 12 Myr, depending upon whether or not it is a member of the $\beta$ Pic moving group (Quast et al. 2000; Kastner et al. 2008). V4046 Sgr has a molecule-rich outer disk ($M_{gas} \sim 110\ M_\oplus$, $M_{dust} \sim 40\ M_\oplus$; Rodriguez et al. 2010); however $\lambda < 10\ \mu$m photometry strongly suggests that the inner disk has been cleared of dust (Jensen & Mathieu 1997). V4046 Sgr was studied as part of the *International Ultraviolet Explorer* (*IUE*) pre-main-sequence star atlas (Johns-Krull et al. 2000), and while $H_2$ emission from the Lyman and Werner levels is strong (see, e.g., Paper I), a mid-IR search for emission from cooler $H_2$ has returned only upper limits (Carmona et al. 2008). The accretion continuum and electron impact excited $H_2$ emission from V4046 Sgr were presented in Paper I.

Our targets were observed with the medium-resolution, far-UV (G130M and G160M) modes of COS (Osterman et al. 2010) during cycle 17, with HN Tau and RECX-11 observed under *HST* program 11616 (PI: G. Herczeg) and V4046 Sgr observed as part of the COS GTO program (PI: J. Green). The total observing times for the three objects were 10.3 ks, 8.2 ks, and 10.1 ks, respectively. In order to achieve continuous spectral coverage and minimize fixed pattern noise, observations in each grating were made with several central wavelength and focal-plane positions (FP-POS). This combination of grating settings covers the $1140\ \text{Å} \leqslant \lambda \leqslant 1760\ \text{Å}$ bandpass for all targets, at a resolving power of $R \approx 18{,}000$.[15] Near-UV imaging target acquisitions were performed through the COS primary science aperture using MIRRORA for HN Tau and MIRRORB for RECX-11 and V4046 Sgr. Table 1 provides a log of the COS observations acquired as part of this study. The data have been processed with the COS calibration pipeline, CALCOS,[16] and combined with the custom IDL co-addition procedure described by Danforth et al. (2010) and Shull et al. (2010).

## 3. RESULTS AND ANALYSIS

### 3.1. Observations of the Carbon Monoxide Fourth Positive System

The three systems discussed here represent the range of CO signatures observed in CTTS spectra during the first year of COS observations. A complete survey of the CO emission observed in the combined GO and GTO observing programs, including spectral modeling to determine CO column densities, CO rotational temperatures, and the spatial distribution of far-UV CO emission for approximately a dozen CTTS disks, is in preparation. Figure 1 shows the spectra in the 1307–1430 Å bandpass. The spectra are displayed on a log scale so that the emission from CO, photo-excited $H_2$, and atomic species can be shown in a single plot. The flux units used in this and subsequent figures are FEFUs[17] (1 FEFU = $1 \times 10^{-15}$ erg cm$^{-2}$ s$^{-1}$ Å$^{-1}$). All three objects show the accretion-generated continuum described in Paper I (see also Calvet & Gullbring 1998 for a detailed theoretically based discussion of the UV–optical spectrum of the accretion shock). The atomic emission lines formed in the active atmosphere (Bouvier et al. 2007), funnel flows (e.g., Muzerolle et al. 2001), and the accretion shock (Günther & Schmitt 2008) are labeled in blue. In this wavelength region, C II λλ1334, 1335 and Si IV λλ1394, 1403 are the strongest atomic species. In the following subsections, we describe the major observational result of this work: the first detection of prominent far-UV emission and absorption features of CO in the spectra of CTTSs.

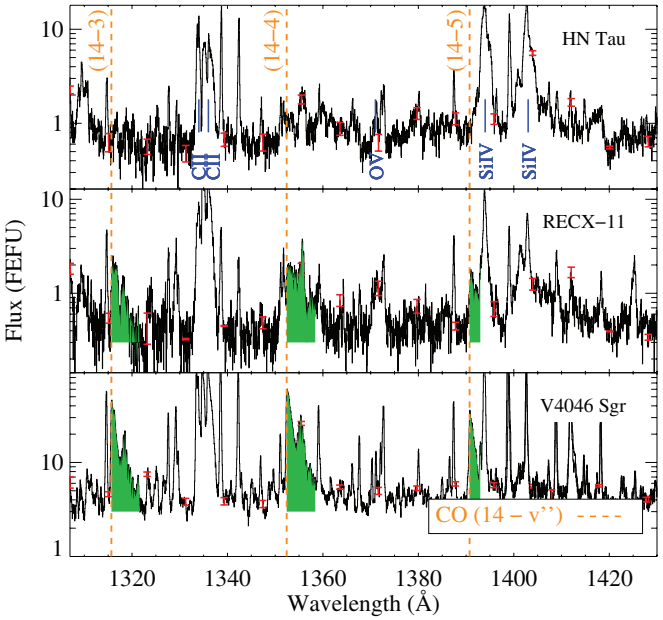


**Figure 1.** 1307–1430 Å spectra of HN Tau, RECX-11, and V4046 Sgr; roughly in order of increasing age from top to bottom. All three spectra show an underlying continuum and emission from atomic species, labeled in blue. The spectrum of V4046 Sgr shows strong CO emission from the $(14 - v'')$ bands in this wavelength interval. We attribute this emission to pumping by stellar Ly$\alpha$ photons. The $(14 - v'')$ bandheads for $v'' = 3$, 4, and 5 are marked with orange dashed lines. Emission lines not labeled as CO or atomic in this wavelength region are produced by photo-excited $H_2$ (Herczeg et al. 2002; Yang et al. 2011). RECX-11 shows less Ly$\alpha$-pumped CO than V4046 Sgr and we do not detect this emission toward HN Tau. The flux is shown on a log scale so the emission from each spectral component can be displayed on a single figure. The flux is plotted in FEFU (≡ femto-erg flux unit, 1 FEFU = $1 \times 10^{-15}$ erg cm$^{-2}$ s$^{-1}$ Å$^{-1}$). Representative error bars on the flux are shown in red.

(A color version of this figure is available in the online journal.)

#### 3.1.1. Lyα Pumping of CO: Selective Rotational Photo-excitation

After the atomic emission lines mentioned above, the next strongest broad emission lines observed are those of CO. The

[15] The COS line-spread function experiences a wavelength dependent non-Gaussianity due to the introduction of mid-frequency wave-front errors produced by the polishing errors on the *HST* primary and secondary mirrors; http://www.stsci.edu/hst/cos/documents/isrs/. We note that for broad emission lines (FWHM $\gtrsim$ 75 km s$^{-1}$), the line-spread function is essentially indistinguishable from Gaussian (France et al. 2010).

[16] We refer the reader to the COS Instrument Handbook for more details: http://www.stsci.edu/hst/cos/documents/handbooks/current/cos_cover.html.

[17] The femto-erg flux unit; see Section 1.1.2 of the Cycle 17 COS Instrument Handbook.

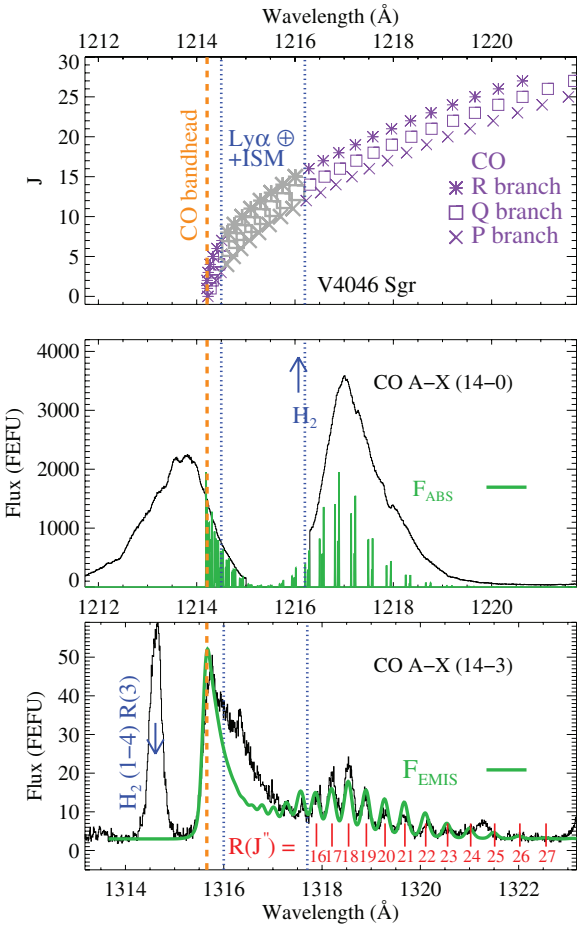


**Figure 2.** Graphical description of the H I Ly$\alpha$ pumping line in V4046 Sgr. The top plot shows the distribution of rotational states (marked with purple stars, squares, and xs) of the CO $A$–$X$ (14–0) band. The rotational states ($J$) corresponding to the center of the stellar+shock Ly$\alpha$ profile are marked by the larger gray symbols; the exciting radiation field at these wavelengths is highly uncertain due to outflow+interstellar absorption and geocoronal emission (labeled "Ly$\alpha \oplus$ + ISM"). We do not attempt to reconstruct the Ly$\alpha$ line profile at these wavelengths; instead we fit a parabola through this region in order to create a continuous pumping profile. In the middle and bottom panels, we show the observed V4046 Sgr Ly$\alpha$ emission line and the (14–3) CO emission band. The (14–0) and (14–3) $A$–$X$ bandheads are marked by the dashed orange lines. The green curves show our model (Section 3.3.1) for the total Ly$\alpha$ flux absorbed by CO (middle) and the fluorescent emission in the (14–3) band (bottom). We find a best-fit model with $N(\mathrm{CO}) = (5.6 \pm 2.3) \times 10^{18}$ cm$^{-2}$ and $T_{\mathrm{rot}}(\mathrm{CO}) = 290 \pm 90$ K. The high rotational level R branch lines are labeled in red on the bottom plot, showing the extent of the observed rotational distribution. The bottom panel shows a strong photo-excited line of $H_2$, $B$–$X$ (1–4) $R(3)$. This line is also pumped by Ly$\alpha$, and we mark the pumping transition wavelength with an "up" arrow in the middle panel.

(A color version of this figure is available in the online journal.)

bright, wide, sawtooth emission features seen in the spectrum of V4046 Sgr (Figure 1, bottom panel and Figure 2, bottom panel) are produced by the $A$–$X$ (14 – $v''$) transitions of CO.[18] The bandheads for the $v'' = 3$, 4, and 5 transitions (1315.7, 1352.4, and 1390.7 Å) are marked. The rotational states of each vibrational band pile up at the bandhead and extend to the red with increasing rotational level.

[18] The quantum numbers $v$ and $J$ denote the ground electronic state ($X^1\Sigma^+$), the numbers $v'$ and $J'$ characterize the CO in the excited ($A^1\Pi$) electronic state, and the numbers $v''$ and $J''$ are the rovibrational levels of the electronic ground state following the fluorescent emission. Absorption lines are described by ($v'$–$v$) and emission lines by ($v'$–$v''$).

**Table 2**
CO Fourth Positive Bands Identified in the Spectra of CTTSs

| Band ID[a] | $\lambda^{b}_{\mathrm{obs}}$ (Å) | Pumping Source | $\lambda_{\mathrm{pump}}$ (Å) |
|---|---|---|---|
| Emission | | | |
| (14–2) | 1280.5 | H I Ly$\alpha$ | 1214–1220 |
| (14–3) | 1315.7 | H I Ly$\alpha$ | 1214–1220 |
| (14–4) | 1352.4 | H I Ly$\alpha$ | 1214–1220 |
| (14–5) | 1390.7 | H I Ly$\alpha$ | 1214–1220 |
| (14–7) | 1472.6 | H I Ly$\alpha$ | 1214–1220 |
| (14–8) | 1516.3 | H I Ly$\alpha$ | 1214–1220 |
| (14–10) | 1610.1 | H I Ly$\alpha$ | 1214–1220 |
| (14–12) | 1713.2 | H I Ly$\alpha$ | 1214–1220 |
| (1–1) | 1560.2 | C I, $e^-$ | 1561 |
| (1–3) | 1669.9 | C I, $e^-$ | 1561 |
| (0–1) | 1597.3 | C IV, C I, $e^-$ | 1544–1550, 1657 |
| (0–2) | 1653.2 | C IV, C I, $e^-$ | 1544–1550, 1657 |
| (0–3) | 1712.4 | C IV, C I, $e^-$ | 1544–1550, 1657 |
| Absorption | | | |
| (0–0) | 1544.4 | ... | ... |
| (1–0) | 1509.8 | ... | ... |
| (2–0) | 1477.6 | ... | ... |
| (3–0) | 1447.4 | ... | ... |
| (4–0) | 1419.0 | ... | ... |
| (6–0) | 1367.6 | ... | ... |
| (7–0) | 1344.2 | ... | ... |
| (8–0) | 1322.1 | ... | ... |

**Notes.**
[a] Transitions are for the $A^1\Pi - X^1\Sigma^+$ CO band system. Band identifications for the emission are labeled ($v'$–$v''$) and absorption lines are labeled ($v'$–$v$).
[b] CO wavelengths are taken from Kurucz (1993).

This (14 – $v''$) progression is pumped through a wavelength coincidence with the stellar Ly$\alpha$ profile. The bandhead of the (14–0) band is at $\lambda = 1214.2$ Å, with higher rotational states extending redward across the H I emission line. This Ly$\alpha$ pumped emission is analogous to the fluorescent $H_2$ cascades pumped by Ly$\alpha$ seen in CTTS spectra (Herczeg et al. 2006). Many emission lines from the Ly$\alpha$-pumped $H_2$ cascade are also visible in the spectra displayed in Figure 1. The CO emission spectrum is present, but less strong in RECX-11, and is not detected in HN Tau. The width of each observed band is 6–7 Å, indicating that rotational excitation as high as $J \approx 30$ is present. It is possible that higher rotational states are populated but not observed in emission because of a lack of Ly$\alpha$ pumping flux redward of 1218 Å.

We detect eight bands of the (14 – $v''$) progression in V4046 Sgr: all bands with $R(0)$ Einstein $A$-values $\gtrsim 2 \times 10^6$ s$^{-1}$ from (14–2) λ1280 to (14–12) λ1713. We detect the complete band sequence with line ratios consistent with the expected branching ratios, demonstrating the solidity of the spectroscopic identifications. We observe (14 – $v''$) bands with $v'' = 2$, 3, 4, 5, 7, and 12 in the spectrum of RECX-11. Bands with $v'' = 1$ and 8–11 are not detected due to small branching ratios and spectral overlap with photo-excited $H_2$. The $v'' = 3$, 4, and 5 bands displayed in Figure 1 are the most readily observable features as these have the largest branching ratios and lie nearest to the peak of the COS spectroscopic sensitivity (Osterman et al. 2010). Table 2 gives a summary of the detected CO emission features.

Figure 2 (bottom) displays the (14–3) band of CO observed in V4046 Sgr in greater detail, as well as the stellar Ly$\alpha$ profile (Figure 2, middle) obtained in the same observations. The CO emission displays rotational structure that reflects the temperature of the CO-bearing gas and the shape of the exciting

**Table 3**
Disk CO Parameters

| Object | Spectral Type | Region | Inclination | Ref. | log($F$(CO))[a] (erg cm$^{-2}$ s$^{-1}$) | log($G_{\rm Ly\alpha}/G_o$)[b] ($a$ = 1 AU) | log($G_{\rm cont}/G_o$) ($a$ = 1 AU) | log$N$(CO) (cm$^{-2}$) | $T_{\rm rot}$(CO) (K) |
|---|---|---|---|---|---|---|---|---|---|
| RECX-11 | K5.5 | $\eta$ Cha | 70° | 1,2,3 | −13.70 | 4.8 | 5.0 | $18.9^{+0.3}_{-0.4}$ | >200K |
| HN Tau | K5 + M4 | Taurus | >40° | 4 | < −14.07 | <4.2 | 6.7 | $17.3^{+0.2}_{-0.3}$ [c] | 500 ± 200[c] |
| V4046 Sgr | K5 + K5 | isolated | 35° | 5,6,7,8 | −12.44 | 5.9 | 5.6 | $18.75^{+0.15}_{-0.25}$ | 290 ± 90 |

**Notes.**
[a] Total integrated CO flux pumped by stellar+accretion shock Ly$\alpha$ photons.
[b] $G_o$ is the average interstellar radiation field evaluated over the 912–2000 Å bandpass ($G_o = 1.6 \times 10^{-3}$ erg cm$^{-2}$ s$^{-1}$; Habing 1968).
[c] Determined from the CO absorption on the line of the sight through the disk.
**References.** (1) Mamajek et al. 1999; (2) Luhman & Steeghs 2004; (3) Lawson et al. 2004; (4) White & Ghez 2001; (5) Quast et al. 2000; (6) Stempels & Gahm 2004; (7) Kastner et al. 2008; (8) Rodriguez et al. 2010.

Ly$\alpha$ radiation field. The intermediate rotational levels are seen to be suppressed (but not absent) in the CO emission spectrum, indicating a self-reversal of the Ly$\alpha$ line profile. This would be expected if the core of the Ly$\alpha$ experiences self-absorption either from an outflow or from neutral hydrogen in the upper disk layers. This is qualitatively similar to the inferred self-reversal of the Ly$\alpha$ profile at the warm $H_2$ layer of the TW Hya disk (Herczeg et al. 2004). We cannot directly measure the core of the Ly$\alpha$ emission line due to absorption from the intervening ISM and outflows, as well as contamination from geocoronal Ly$\alpha$ that fills the COS aperture (see Section 3.2). The region over which geocoronal and interstellar Ly$\alpha$ contaminate the V4046 Sgr spectrum is marked with dotted lines in Figure 2 (middle). We calculate the total Ly$\alpha$-pumped CO emission ($F$(CO), in units of erg cm$^{-2}$ s$^{-1}$) by integrating the (14–3) band ($F$(14–3)) over the 6 Å redward of the bandhead, subtracting the continuum contribution over the same region. The total CO emission is $F$(CO) = $F$(14–3)/$B$(14–3), where $B$(14–3) is the branching ratio for emission into the $v'' = 3$ level. The total Ly$\alpha$-pumped CO fluxes are listed in Table 3.

Figure 2 also shows a complementary example of Ly$\alpha$ pumped $H_2$ emission from the V4046 Sgr disk, the $B$–$X$ (1–4) $R$(3) [$\lambda_{\rm rest}$ = 1314.62 Å] line, which is pumped by the coincidence of Ly$\alpha$ with the (1–2) $P$(5) [$\lambda_{\rm rest}$ = 1216.07 Å] transition. The absorbing transition is marked with an "up" arrow, and the emission line is marked with a "down" arrow.

### 3.1.2. Other CO Emission Bands

We also identify CO $A$–$X$ emission excited through other routes, most notably the (0–1) λ1597 and (0–3) λ1712 bands in all three systems (Figure 3). These emissions may be attributed to pumping by C IV, whose flux overlaps with the $A$–$X$ (0–0) band because of the width of the C IV line profile and the broad rotational state population of the CO. Alternatively, CO excitation by non-thermal electrons (Beegle et al. 1999), analogous to collisionally excited $H_2$ emission (Bergin et al. 2004; Paper I), is an intriguing possibility. In disks orbiting stars with strong photospheric/chromospheric carbon emission, C I λ1657 may contribute to the pumping through a coincidence with the (0–2) CO band. The analysis and modeling of this emission is ongoing, and a more complete analysis will be described in the larger CO survey. As noted in Paper I, the (0–1) λ1597 feature is a major source of spectral confusion for studies of electron impact excited $H_2$ in CTTS observations at low spectral resolution (e.g., Ingleby et al. 2009). $H_2$ excited by electrons with energies, $E_e$, $\gtrsim$ 15 eV, displays a characteristic gap in its emission spectrum at 1600 Å. Thus, in order to use the 1600 Å flux to determine the mass surface density of the inner

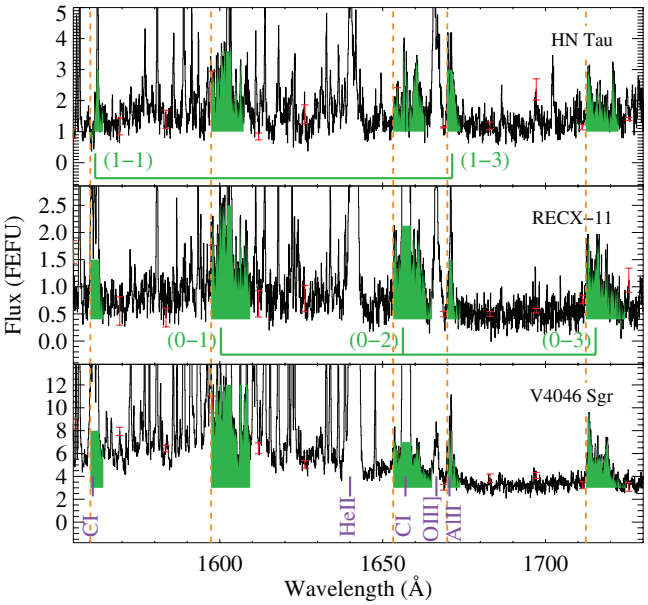


**Figure 3.** Montage of the CO $A$–$X$ emission in the 1560–1730 Å wavelength interval. The flux attributable to CO is shaded in green. The emission at 1713 Å is a combination of the (14–12) and (0–3) progressions in V4046 Sgr and RECX-11. The 1713 Å lines are an important signpost for the presence of CO in the spectrum because this wavelength region is free of blending with $H_2$. CO bandheads are marked with dashed orange lines, and atomic features are labeled in purple. CO line identifications and possible excitation mechanisms are presented in Table 2. All other emission features not identified as CO or atomic emission in this figure are photo-excited and collisionally excited $H_2$ (Herczeg et al. 2002; Paper I).
(A color version of this figure is available in the online journal.)

molecular disk, the contribution from CO must be accounted for. This is complicated by the wealth of stronger photo-excited $H_2$ lines in the $\lambda \leqslant 1650$ Å bandpass. The 1712–1720 Å spectrum, which is predominantly emission from the CO (0–3) and (14–12) bands, is free of Lyman and Werner band $H_2$ lines (Abgrall et al. 1993) and can be used as a signpost for CO in the emission spectrum. We also detect spectral features coincident with the (1–1) λ1560 and (1–3) λ1670 bands. The latter is seen in the spectrum of HN Tau presented in Figure 3. The (1–1) band is coincident with stellar C I λ1561 and we propose that the (1–$v''$) emission could be partially excited by C I photons.

### 3.1.3. CO Fourth Positive Absorption Bands

We detect CO absorption bands in the spectrum of HN Tau. The CO absorption bands arise from the ground vibrational state ($v'$–0) and are seen superimposed on the continuum produced

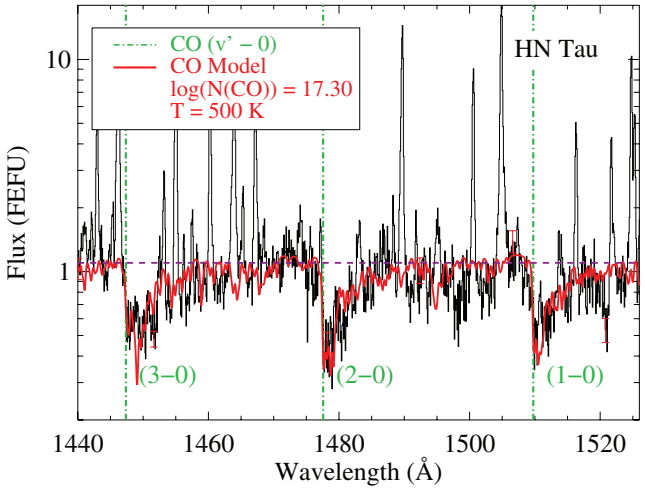


**Figure 4.** HN Tau spectrum in the 1440–1526 Å bandpass is shown in black. Fitting the CO transmission spectrum (fit displayed as the red line), we find $N(\mathrm{CO}) = 2 \pm 1 \times 10^{17}$ cm$^{-2}$, $T_{\mathrm{rot}}(\mathrm{CO}) = 500 \pm 200$ K, suggesting that the absorbing gas is in the warm inner disk. The $(v' - 0)$ absorption bands suggest a line of sight through much of the disk and thus a high disk inclination because the absorption bands are not observed in V4046 Sgr or RECX-11, whose CO emission suggests even higher column densities. The continuum level has been set to 1.2 FEFU over the 1440–1526 Å band for this fitting.

(A color version of this figure is available in the online journal.)

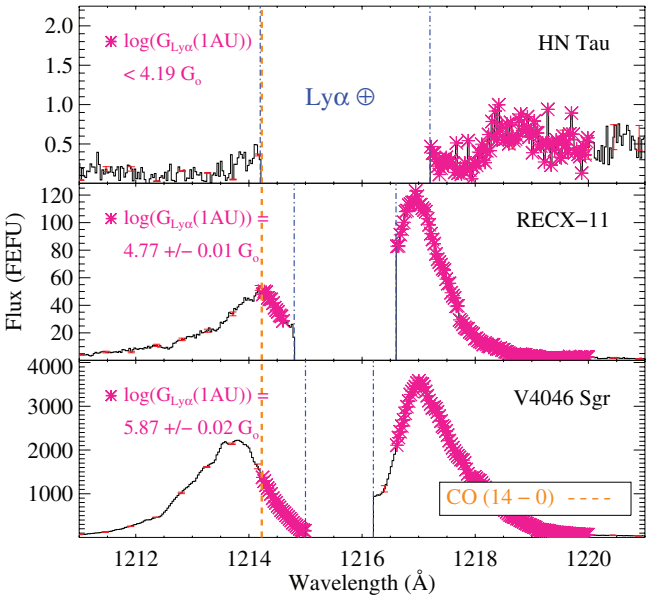


**Figure 5.** Strength of the *observed* Ly$\alpha$ emission across the CO (14–0) band is proportional to the strength of the resultant fluorescence (compare, e.g., with Figure 1). We have calculated the strength of the radiation field available to be absorbed at 1 AU (in units of the Habing flux, $G_o = 1.6 \times 10^{-3}$ erg cm$^{-2}$ s$^{-1}$), at wavelengths unaffected by geocoronal emission (magenta stars). The integrated flux level is shown at the upper left of each panel and in Table 3. The inner regions of the HN Tau profile are still contaminated by the wings of the geocoronal H I, thus only an upper limit to the Ly$\alpha$ emission can be determined. The position of the (14–0) bandhead is marked with the dashed orange line.

(A color version of this figure is available in the online journal.)

by the accretion shock. Figure 4 shows the absorption spectrum of HN Tau from 1440 to 1526 Å where the strongest absorbers ($v' = 1$–3) are observed. The absorption profile can be explained by a viewing geometry where we are looking through an optically thick region of a high-inclination system, though not all high-inclination disk systems in the Taurus–Auriga region show warm CO absorption signatures (e.g., DF Tau). As discussed below, the wealth of $H_2$ and atomic emission lines makes a determination of the continuum level very challenging, so we assume a flat continuum level in this region of $F_\lambda = 1.2 \times 10^{-15}$ erg cm$^{-2}$ s$^{-1}$ Å$^{-1}$ ($\equiv$ 1.2 FEFU). Assuming this continuum level in the 1440–1526 Å bandpass, each absorption band has a width of 10–15 Å, indicating a high degree of rotational excitation. For comparison, resolved absorption bands of cool CO ($T_{\mathrm{rot}}(\mathrm{CO}) \approx 4$ K) characteristic of diffuse and translucent interstellar material have typical widths $\lesssim 0.5$ Å (Burgh et al. 2007). The observed band widths imply that the CO rotational excitation temperature in HN Tau absorbing gas must be greater than a few $\times 10^2$ K. Table 2 lists the absorption bands observed in HN Tau.

### 3.2. Ly$\alpha$ and the Far-UV Continuum

Figure 5 displays the Ly$\alpha$ profiles of the three systems. COS is a slitless spectrograph, and contamination from geocoronal H I emission renders unusable the inner 1.2–3.0 Å of the Ly$\alpha$ profile. We can, however, measure the broad wings of the stellar+accretion Ly$\alpha$ profile, where the majority of the CO absorption takes place. In order to quantify the strength of the available Ly$\alpha$ pumping flux, we integrate each of the Ly$\alpha$ profiles from the CO (14–0) bandhead ($\lambda_{\mathrm{rest}} = 1214.22$ Å) to 1220 Å, masking out the airglow emission. The extinction toward RECX-11 and V4046 Sgr is relatively small (Luhman & Steeghs 2004; Stempels & Gahm 2004), and from the observed Ly$\alpha$ profiles we estimate neutral hydrogen column densities of $\log(N(\mathrm{H})) < 19.5$ cm$^{-2}$, corresponding to $E(B - V) < 0.006$ for typical interstellar gas-to-dust ratios (Bohlin et al. 1978). No dereddening was performed for V4046 Sgr or RECX-11. The extinction to HN Tau is somewhat uncertain, so we adopt the average of the extinction to the individual components ($A_V \approx 1.0$; White & Ghez 2001), and deredden the spectrum assuming the Cardelli et al. (1989) curve for $R_V = 4.0$ (Mathis 1990). This value may underestimate the reddening associated with HN Tau; however, this value does not impact any of the CO parameters derived in Section 3.3.

We calculate the strength of the Ly$\alpha$ radiation field ($G_{\mathrm{Ly}\alpha}$) at 1 AU from the central stars in units of the interstellar ultraviolet radiation field (Habing 1968). While this treatment does not make any correction for the ISM or the geometry of the inner disk, we find that the flux of the Ly$\alpha$-pumped CO emission is proportional to the strength of the Ly$\alpha$ profile as observed at Earth (Columns 6 and 7 in Table 3). We note that the same is not necessarily true for $H_2$ (e.g., we see numerous fluorescent $H_2$ emission lines in the spectrum of HN Tau without directly observing strong Ly$\alpha$ emission). We have not attempted to reconstruct the stellar Ly$\alpha$ profile here. We can compare the observed Ly$\alpha$ emission strength with that of the continuum, $G_{\mathrm{cont}}$. Following the method described in Paper I, we have measured the continuum spectra of the three systems. These data are shown in Figure 6, where the flux units have been scaled to the local radiation field strengths at 1 AU from their host stars. The integrated 912–2000 Å fluxes are presented in Table 3. We find that the observed $G_{\mathrm{Ly}\alpha}$ and $G_{\mathrm{cont}}$ are comparable for V4046 Sgr and RECX-11, while the strength of the UV continuum is more than two orders of magnitude greater than the observed (unreconstructed) Ly$\alpha$ flux in HN Tau. The large difference between the Ly$\alpha$ and accretion continuum observed in HN Tau is most likely attributable to strong H I attenuation on the sightline (disk + interstellar) to HN Tau. The Ly$\alpha$ photons are scattered out of our line of sight while passing through the disk, whereas the continuum emission is only attenuated by

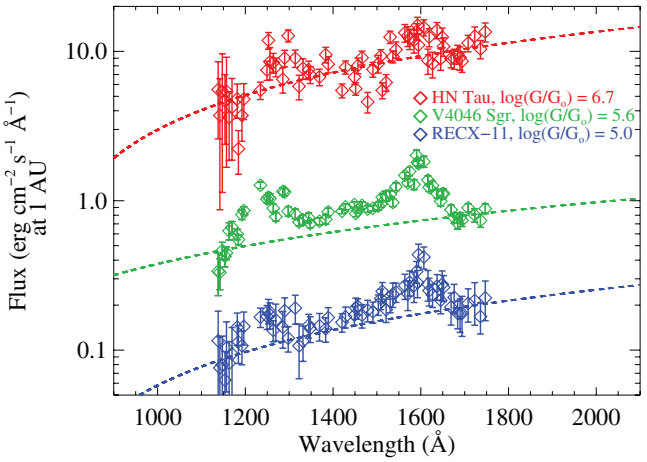


**Figure 6.** FUV accretion continuum in our three targets. The continuum is measured in 0.75 Å bins between stellar and disk emission lines (Paper I). The binned continuum measurements are shown as diamonds. The HN Tau data have been corrected for interstellar reddening, adopting the average extinction of the HN Tau system (White & Ghez 2001), while RECX-11 and V4046 Sgr are consistent with $E(B-V) < 0.006$ (Section 3.2) and no reddening correction is performed. The dashed lines are fits to the spectra in regions that are free of contamination from photo-excited $H_2$ emission ($\lambda < 1180$ Å and $\lambda > 1660$ Å). The smooth emission above the dashed lines is attributable to collisionally excited $H_2$ (Bergin et al. 2004; Paper I). The continuum fits are extrapolated over the 912–2000 Å bandpass, and the integrated fluxes are listed in the legend and Table 3.

(A color version of this figure is available in the online journal.)

dust grains. The grain opacity is several orders of magnitude less than the line-center atomic hydrogen opacity (Fogel et al. 2011). Additionally, grain growth acts to reduce the UV dust opacity (Vasyunin et al. 2011), making the continuum emission more readily observable through the disk.

### 3.3. Analysis

#### 3.3.1. Lyα Pumping of CO

We constructed a simple model to estimate the properties of the photo-excited CO population (the CO column density on the star-disk sightline, $N$(CO), and the CO rotational temperature, $T_{\rm rot}$(CO)) in the inner disks of V4046 Sgr and RECX-11. We used the Dunham coefficients from George et al. (1994) to calculate the ground electronic state CO term values. The ground state energy is used to create a population distribution ($P(v = 0, J)$) that is characterized by $T_{\rm rot}$(CO). We then compute the absorption cross-sections for the $A$–$X$ (14–0) transitions using the Einstein $A$-values and wavelengths from Kurucz (1993). The CO optical depth is $\tau_\lambda = N({\rm CO})P(0, J)\sigma_\lambda$. The total absorbed flux is then

$$I_\lambda = I_\lambda^o(1 - e^{-\tau_\lambda}), \quad (1)$$

where $I_\lambda^o$ is the incident Lyα radiation field. Our model does not make an assumption about the geometry of the absorbing gas. Because the transition probabilities of the (14–0) absorption lines are intrinsically small ($\sim 10^4$ s$^{-1}$), optical depth effects do not dominate the uncertainty on the total absorbed/emitted flux. A spatial distribution where the CO is concentrated in one dense parcel at the inner edge of the molecular gas disk cannot be distinguished from a more tenuous distribution of CO across a larger disk surface in our approach.

The emitted flux is determined by the branching ratios to the various rovibrational levels of the $X^1\Sigma^+$ ground electronic state. The branching ratios for a given transition $(A^1\Pi,v',J') \rightarrow (X^1\Sigma^+,v'',J'')$ are subject to the appropriate dipole selection rules and the Franck–Condon factors. The crucial input for this simplified model of the observed CO emission is $I_\lambda^o$, the stellar+shock Lyα profile as seen by the CO in the disk. The shape of this profile will depend strongly on the intervening neutral hydrogen in the protostellar outflow and disk atmosphere. The intervening H I absorbers will not only determine the absolute level of the incident radiation field, but also the wavelengths of accessible pumping photons. For simplicity, we assume that the observed Lyα profile, not including the region near the line center where interstellar and geocoronal H I complicate the profile, is representative of the Lyα seen by the CO. In order to create a continuous Lyα pumping profile, we fit a parabola across the spectral region where geocoronal emission has been removed.

We illustrate the modeling process for V4046 Sgr in Figure 2. In the top panel, we show the wavelength distribution of rotational states in the (14–0) band. In the middle panel, we show the stellar Lyα profile, with the flux absorbed by CO in green. We note that the CO absorption is not seen against the Lyα profile, unlike the $H_2$ absorption profiles discussed by Yang et al. (2011). The lack of observable CO absorption on the Lyα profile is most likely due to a combination of the low inclination of the system, the relatively small transition probabilities from the ground vibrational level to $v' = 14$, and the moderate resolving power of COS. The absorbed flux is redistributed among the $v''$ levels during the fluorescent cascade, and we show the (14–3) emission band in the lower panel of Figure 2. The model emission is shown in green. States affected by uncertainties in the Lyα profile are marked in gray. Figure 2 shows that the model underpredicts the observed CO emission for the rotational states that are pumped by the Lyα line center. This indicates that the illumination by the Lyα line center is significant in the inner disk, consistent with the observation of strong $H_2$ emission pumped through the $B$–$X$ (1–2) $R(6)$ 1215.73 Å and (1–2) $P(5)$ 1216.07 Å absorbing transitions. In the larger CTTS CO survey in preparation, we will present a more sophisticated CO fluorescence model, including a self-consistent reconstruction of the Lyα profile.

$N$(CO) in the ground electronic state is determined by the amount of absorption required to produce the observed fluorescent emission in our approach. For a completely optically thin parcel of gas, $N$(CO) is degenerate with the covering fraction of CO in the disk. The rotational excitation temperature controls the rotational-state population of the absorbing molecules, which we constrain by observing the distribution of emission lines in highly excited rotational levels ($J'' > 10$). We searched a grid of column density and temperatures for the best fit to the COS observations. Exploring regions of parameter space that are inconsistent with the observations allows us to place error bars on $N$(CO) and $T_{\rm rot}$(CO). Figure 7 shows synthetic CO spectra for the 1$\sigma$ error bars of $T_{\rm rot}$(CO) to illustrate the model dependence on the temperature. Values for $N$(CO) that are outside of the error bars predict too much or too little total CO flux, while values for $T_{\rm rot}$(CO) that are outside of the error bars either do not predict the high-$J$ CO lines seen in the data or predict many more lines than are observed. We note that the highest rotational levels may not be thermalized due to their larger critical densities ($n({\rm H})_{\rm crit} \gtrsim 10^5$ cm$^{-3}$ for $J > 10$). This effect would cause our $T_{\rm rot}$(CO) to systematically underestimate the kinetic temperature of the CO-bearing gas. Due to the much stronger relative contribution of geocoronal Lyα and the lower signal-to-noise ratio (S/N) of the RECX-11 spectrum, we were

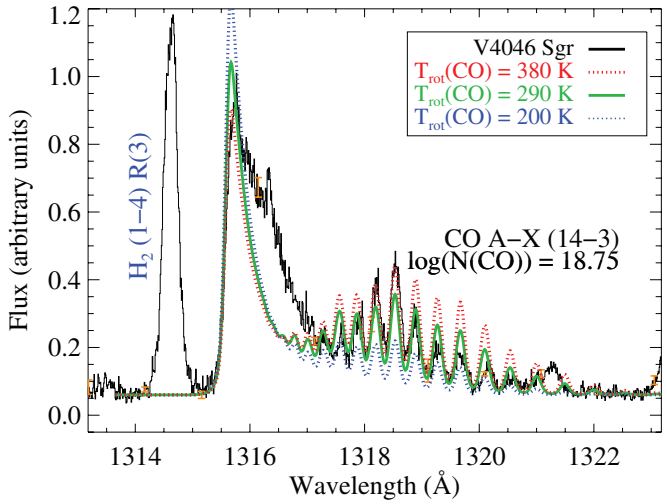


**Figure 7.** CO models for the $T_{\rm rot}$(CO) consistent with the COS observations of V4046 Sgr (shown in black, see Figure 2). There is a slight $N$–$T_{\rm rot}$ degeneracy in the model fits, though in general, $N$(CO) controls the output flux and $T_{\rm rot}$(CO) controls the population of the high-$J$ states seen in the CO emission profiles. The best-fit models find $N(\mathrm{CO}) = (5.6 \pm 2.3) \times 10^{18}$ cm$^{-2}$ and $T_{\rm rot}(\mathrm{CO}) = 290 \pm 90$ K. The model underpredicts the observed flux between 1316 and 1317 Å due to uncertainties in the exciting Ly$\alpha$ emission profile (Section 3.3.1). (A color version of this figure is available in the online journal.)

only able to use the red side of the pumping profile and thus higher rotational levels to constrain the CO parameters in this system. The uncertainties on $N$(CO) are correspondingly larger for RECX-11. With this simple approach, we can only set a lower limit on the rotational excitation temperature because the red-wing of the RECX-11 Ly$\alpha$ profile does not excite CO with $J \gtrsim 20$, so higher rotational temperatures cannot be excluded.

Following this modeling procedure, we determine that the Ly$\alpha$-pumped CO emission observed in V4046 Sgr and RECX-11 has column densities of $N(\mathrm{CO}) = (5.6 \pm 2.3) \times 10^{18}$ cm$^{-2}$ and $(8 \pm 4) \times 10^{18}$ cm$^{-2}$, respectively. The rotational excitation temperatures for V4046 Sgr and RECX-11 are $T_{\rm rot}(\mathrm{CO}) = 290 \pm 90$ K and >200 K. A velocity broadening of 20 km s$^{-1}$ was applied to the emission spectrum to match the width of the high-$J$ lines observed in the V4046 Sgr data. Due to its large molecular mass, the thermal width of CO lines is relatively small ($v_{\rm therm} < 1$ km s$^{-1}$ for $T_{\rm rot}(\mathrm{CO}) < 1700$ K), so the velocity broadening is almost certainly dominated by a combination of turbulence and Keplerian rotation of the CO-bearing gas. It should be noted that this is smaller than the 52 km s$^{-1}$ line width observed in the sample of 13 photo-excited $H_2$ lines presented in Paper I; however a direct comparison of these values should be made with caution due to blending between the R, P, and Q branches as well as uncertainties in the CO wavelengths for the high-$J$ ($14 - v''$) lines.

#### 3.3.2. CO Absorption

We can also use the CO ($v' - 0$) absorption spectrum to constrain the column density and temperature of the CO in high-inclination disks. We have created synthetic optical depth spectra for the attenuation of UV photons through a screen of CO molecules to compare with the HN Tau spectra. These optical depths assume a turbulent velocity (0.1 km s$^{-1}$) and are characterized by a column density and rotational temperature. The model CO absorption spectrum is compared to the observed CO absorption bands in Figure 4. There are two main points of uncertainty with this treatment of the absorption lines: (1) the continuum placement and (2) the S/N of the data. There are many emission lines from photo-excited $H_2$ and hot gas in the far-UV spectra of CTTS that make a determination of the continuum level challenging. Continuum placement is critical for profile fitting of molecular absorption spectra (Sonnentrucker et al. 2007). In the case of HN Tau, uncertainties on the continuum level complicate measurements of high-$J$ absorption (and thus $T_{\rm rot}$). The flux in the HN Tau spectra in the region of CO absorption is $F_\lambda \lesssim 1$ FEFU, so structure in the line profiles is lost in the noise. Despite these challenges, we can use the ($v' - 0$) absorption bands to constrain the column density and temperature to $N(\mathrm{CO}) = (2 \pm 1) \times 10^{17}$ cm$^{-2}$ and $T_{\rm rot}(\mathrm{CO}) = 500 \pm 200$ K.

## 4. DISCUSSION OF FAR-UV CO AND $H_2$ EMISSION FROM THE INNER DISK

### 4.1. The Molecular Excitation and Spatial Distributions

We have used the combination of sensitivity and spectral resolution afforded by *HST*-COS to isolate and characterize CO emission in the far-UV spectra of protoplanetary disks for the first time. Our values for the rotational temperature are in the range of a few hundred kelvin, and if we assume that the CO population is in thermal equilibrium with the stellar radiation, this places the CO at an orbital distance of ~0.2–2 AU in our targets. Additionally, CO rotational temperatures in this range suggest that the photo-excited CO we observe may not be related to the CO traced through the $\lambda \sim 4.7\,\mu$m fundamental bands, although this correlation will require more study. In general, we find that the fluorescent CO emission detected here arises in gas that is somewhat less energetic than traced by $M$-band CO emission, which is characterized by temperatures of ~1000 K (Najita et al. 2003). It should be noted however that our results are roughly consistent with the rotational temperatures measured from a sample of VLT-CRIRES spectra of protoplanetary disks (Bast et al. 2011). These authors find a decoupling of the rotational and vibrational populations in a small subsample of CTTSs with large accretion rates, suggesting that the ground state vibrational populations are influenced by non-thermal UV photo-excitation (see also Brittain et al. 2007). Interestingly, an analogous process may be occurring in the $H_2$ population of the inner disk, namely, that excitation by non-thermal processes such as photo-excitation (Ardila et al. 2002) and excitation by photoelectrons (Bergin et al. 2004; Paper I) could lead to an effective vibrational temperature that is significantly higher than the rotational or kinetic temperature of the molecules.

At the temperatures and densities characteristic of the inner gas disks, the small critical densities of the pure rotational transitions of $H_2$ ($n_{\rm crit} < 2000$ cm$^{-3}$ for $J'' \leqslant 3$ and $T_{\rm rot}(\mathrm{H_2}) \gtrsim 1000$ K; Mandy & Martin 1993) should make them excellent tracers of the kinetic temperature. However, due to their very small transition probabilities, $H_2$ rotational lines have proven very difficult to observe in circumstellar disk environments (Pascucci et al. 2006; Lahuis et al. 2007; Bitner et al. 2008; Carmona et al. 2008). Larger aperture and source sizes allowed for robust detections of the $H_2$ rotational spectrum in photodissociation regions (PDRs) with the *Spitzer*-IRS (e.g., Fleming et al. 2010). PDRs and the inner regions of protoplanetary disks display qualitative similarities: a strong UV radiation field photodissociating and partially ionizing a molecular medium (Gorti & Hollenbach 2002, 2009). Far-UV observations of photo-excited $H_2$ in PDRs show a decoupling of the vibrational and rotational

temperatures, with vibrational temperatures of order 2000–3000 K (France et al. 2005). Mid-IR observations of these same regions with *ISO*, *Spitzer*, and ground-based spectrographs reveal that the rotational temperatures of these regions are typically 300–900 K (Habart et al. 2004; Allers et al. 2005; France et al. 2007; Fleming et al. 2010). This is the same qualitative behavior observed in CO observations of CTTS disks, and we argue that the UV-pumping process can influence both the CO and $H_2$ level populations in these systems.

The similarity of the physical conditions in the $H_2$ and CO emitting regions, particularly the fact that both species show photoexcitation from the Ly$\alpha$ line core (Section 3.3.1), naively implies that they are co-spatial. Deep far-UV spectroscopy allows us to observe both molecular species from a common physical origin in a single observation. The argument we present here is somewhat qualitative; the physical state and composition of the molecular inner disk is a complicated balance of radiative excitation by continuum and line photons, collisional population of the rovibrational levels of the ground electronic state, and non-thermal processes such as collisions with photoelectrons. A rigorous treatment of the distribution of photo-excited and collisionally excited molecular populations is beyond the scope of this work. More complex theoretical models that predict both the UV and submillimeter/millimeter wavelength line fluxes are needed for future studies of the warm molecular phase of protoplanetary disks.

The fact that the Ly$\alpha$ pumping of CO proceeds at all is a strong argument for a disk surface origin of the CO emission. In the absence of a local source of Ly$\alpha$ photons within the disk, our observations strongly suggest that both the CO and $H_2$ are shielded by very little neutral hydrogen. If one assumes a standard dark cloud $N(\mathrm{CO})/N(\mathrm{H_2})$ ($\equiv \mathrm{CO/H_2} \approx 10^{-4}$) conversion factor and a molecular fraction of 0.67, CO column densities of order $10^{18}$ cm$^{-2}$ would be located in a medium with $N(\mathrm{H}) \sim 10^{22}$ cm$^{-2}$. This is clearly not feasible because the average neutral hydrogen optical depth at the wavelengths required to excite the observed CO fluorescence ($\langle \tau_{\mathrm{H\,I}}(1210\text{–}1220\,\text{Å}) \rangle$) would be $>10^7$ at $N(\mathrm{H}) \sim 10^{22}$ cm$^{-2}$. H I column densities larger than $\sim 10^{20}$ cm$^{-2}$ are incompatible with the observed CO emission. This implies that CO/H $> 10^{-2}$ in the CO emitting region and argues strongly for an origin at the disk surface.

### 4.2. The $CO/H_2$ Ratio in the Inner Disk

Having demonstrated that the CO and $H_2$ may be sampling the same distribution of inner disk gas, we can evaluate the $\mathrm{CO/H_2}$ ratio, $X_{\mathrm{CO}}$ (Liszt et al. 2010), in the inner disk. The photo-excited $N(\mathrm{H_2})$ in the inner disk of CTTSs has been measured in the range $10^{18}$–$10^{19}$ cm$^{-2}$ (Herczeg et al. 2004; and extrapolating the high excitation $H_2$ column densities from Ardila et al. 2002). This is essentially identical to the column density of $H_2$ excited by electron impact in CTTS disks (Ingleby et al. 2009; Paper I), although it is not yet clear whether or not collisionally excited gas traces the photo-excited population. Thus, we suggest that the $\mathrm{CO/H_2}$ ratio in the disk surface at terrestrial planet forming radii is of order unity ($N(\mathrm{CO})/N(\mathrm{H_2}) \sim 1$), far from the dense cloud value of $10^{-4}$ that is typically assumed.

$\mathrm{CO/H_2} \sim 1$ suggests considerable evolution from the dense cloud from which the system formed, and may represent a transitional phase between the interstellar and cometary environments ($\mathrm{CO/H_2} \sim 30$; Lupu et al. 2007) where water ice regulates the gas phase abundances of both molecules. We suggest two possible processes that could drive the $\mathrm{CO/H_2}$ ratio toward the observed levels. Photoevaporation and/or collisions of large grains/planetesimals have been suggested as sources for maintaining a gas-phase carbon abundance in debris disk systems (Vidal-Madjar et al. 1994; Lecavelier des Etangs et al. 2001; Chen & Jura 2003). We suggest that this second-generation CO could be produced in collisions in the dust disk region and transported to the surface of the inner disk by mass-flow induced by photo-evaporation (Gorti & Hollenbach 2009).

$H_2$ could be selectively dissociated by the radiation field present in the inner disk. $H_2$ can be photodissociated by a two-step process where a photon is absorbed into the Lyman band system followed by emission into the vibrational continuum, when $v'' > 14$ (Stecher & Williams 1967). For molecules exposed to the far-UV continuum of an O or B star, the dissociation probability ($p_{\mathrm{diss}} = A_{\mathrm{cont}}/A_{\mathrm{TOT}}$, the ratio of the transition probability to the vibrational continuum compared with the total transitional probability from a given upper state) is 0.1–0.15. Warm $H_2$ will have absorption out of the high-$J$ lines of the Lyman (0–0) band at wavelengths as long as 1140–1150 Å, and multiple pumping effects can introduce additional absorption opacity at longer wavelengths. The predissociating transitions of CO all require photons of $\lambda \lesssim 1076$ Å (starting with the $E$–$X$ bands; van Dishoeck & Black 1988). Predissociation of CO through the $A$–$X$ bands is negligible (see, e.g., the $A$–$X$ system parameters measured by Le Floch et al. 1987). We have shown that the accretion-powered far-UV continuum is decreasing from 1150 to 1076 Å (Figure 6), indicating that $H_2$ molecules in circumstellar disks may be selectively dissociated by continuum photons more readily than in interstellar clouds. However, the dominant mechanism for $H_2$ dissociation in the inner disk is most likely the huge flux of Ly$\alpha$ photons produced by the star+accretion shock. The Lyman band $H_2$ transitions in the range 1214–1217 Å have very low dissociation probabilities. However, there are several Werner band lines in that region with both large radiative rates into the upper level and large rates to the continuum ($p_{\mathrm{diss}} \sim$ 0.07–0.17). Furthermore, there are several strong transitions ($A_{\mathrm{TOT}} > 10^8$ s$^{-1}$) to the $B'$ electronic levels with $p_{\mathrm{diss}} >$ 0.5 coincident with Ly$\alpha$. A complete characterization of the abundances of CO and $H_2$ in the inner dust disk will require additional modeling, but mechanisms to produce high $\mathrm{CO/H_2}$ ratios are available.

Alternatively, there may be a geometrically thin population of $H_2$ characterized by kinetic temperatures of order 2500 K (Herczeg et al. 2004). If this population dominates the observed $H_2$ fluorescence, then the CO is tracing a cooler bulk distribution where the $N(\mathrm{H_2})$ may be higher. In this case, a direct comparison between the two molecules breaks down. Finally, the $\mathrm{CO/H_2}$ ratio observed in the inner disk does not necessarily have any bearing on the $\mathrm{CO/H_2}$ ratio in the more quiescent outer disk probed by millimeter-wave CO measurements. However, our results suggest that the traditional assumption of a dense cloud $X_{\mathrm{CO}}$-conversion factor for determining the total molecular mass of a protoplanetary disk may not be correct, and more work should be focused on determining an environmentally dependent $X_{\mathrm{CO}}$-conversion factor.

## 5. SUMMARY

We have presented the first far-UV detections of CO emission and absorption from the planet-forming region of CTTS disks. We detect for the first time Ly$\alpha$-pumped CO emission bands in V4046 Sgr and RECX-11. The far-UV emitting CO is characterized by $N(\mathrm{CO}) \sim 10^{18}$–$10^{19}$ cm$^{-2}$, with rotational

excitation temperatures of $\gtrsim$300 K. We clearly detect warm CO in absorption against the accretion continuum in HN Tau with $N(\mathrm{CO}) \sim 2 \times 10^{17}$ cm$^{-2}$, $T_{\mathrm{rot}}(\mathrm{CO}) \sim 500$ K. These data provide direct evidence for the influence of UV photons on CO-rich inner disks. We compare these results with observations of photo-excited and collisionally excited $H_2$ to determine that the CO and $H_2$ populations observed with far-UV spectroscopy may be co-spatial. This suggests that the CO/$H_2$ ratio in the inner regions of protoplanetary disks is of order unity, possibly due to a combination of replenishment of gas-phase CO and selective photodissociation of $H_2$. We are in the process of assembling a larger survey of photo-excited CO emission in protoplanetary disk targets. This work, which will present more sophisticated modeling of the Ly$\alpha$ radiation field and CO fluorescence, will be used to compare the physical characteristics of the UV-emitting CO with system parameters such as age, mass accretion rate, and disk mass.

K.F. thanks Roxana Lupu for enjoyable discussions regarding the far-UV spectrum of CO. This work was support by NASA grants NNX08AC146 and NAS5-98043 to the University of Colorado at Boulder and STScI grants to program GO-11616.

## REFERENCES


Abgrall, H., Roueff, E., Launay, F., Roncin, J. Y., & Subtil, J. L. 1993, A&AS, 101, 273
Allers, K. N., Jaffe, D. T., Lacy, J. H., Draine, B. T., & Richter, M. J. 2005, ApJ, 630, 368
Andrews, S. M., & Williams, J. P. 2005, ApJ, 631, 1134
Ardila, D. R., Basri, G., Walter, F. M., Valenti, J. A., & Johns-Krull, C. M. 2002, ApJ, 566, 1100
Bartoe, J., Brueckner, G. E., Sandlin, G. D., Vanhooster, M. E., & Jordan, C. 1978, ApJ, 223, L51
Bast, J., Brown, J., Herczeg, G., van Dishoek, E., & Pontoppidan, K. 2011, A&A, 1, 0
Beegle, L. W., Ajello, J. M., James, G. K., Dziczek, D., & Alvarez, M. 1999, A&A, 347, 375
Bergin, E., et al. 2004, ApJ, 614, L133
Bethell, T., & Bergin, E. 2009, Science, 326, 1675
Bitner, M. A., et al. 2008, ApJ, 688, 1326
Bohlin, R. C., Savage, B. D., & Drake, J. F. 1978, ApJ, 224, 132
Bouvier, J., Alencar, S. H. P., Harries, T. J., Johns-Krull, C. M., & Romanova, M. M. 2007, in Protostars and Planets V, ed. B. Reipurth, D. Jewitt, & K. Keil (Tucson, AZ: Univ. Arizona Press), 479
Brittain, S. D., Simon, T., Najita, J. R., & Rettig, T. W. 2007, ApJ, 659, 685
Brown, A., Jordan, C., Millar, T. J., Gondhalekar, P., & Wilson, R. 1981, Nature, 290, 34
Burgh, E. B., France, K., & McCandliss, S. R. 2007, ApJ, 658, 446
Calvet, N., & Gullbring, E. 1998, ApJ, 509, 802
Cardelli, J. A., Clayton, G. C., & Mathis, J. S. 1989, ApJ, 345, 245
Carmona, A., et al. 2008, A&A, 477, 839
Carpenter, K. G., Robinson, R. D., Wahlgren, G. M., Linsky, J. L., & Brown, A. 1994, ApJ, 428, 329
Carr, J. S., & Najita, J. R. 2008, Science, 319, 1504
Carr, J. S., Tokunaga, A. T., & Najita, J. 2004, ApJ, 603, 213
Chen, C. H., & Jura, M. 2003, ApJ, 582, 443
Danforth, C. W., Keeney, B. A., Stocke, J. T., Shull, J. M., & Yao, Y. 2010, ApJ, 720, 976
Durrance, S. T. 1981, J. Geophys. Res., 86, 9115
Dutrey, A., Guilloteau, S., Duvert, G., Prato, L., Simon, M., Schuster, K., & Menard, F. 1996, A&A, 309, 493
Federman, S. R., Glassgold, A. E., Jenkins, E. B., & Shaya, E. J. 1980, ApJ, 242, 545
Feldman, P. D., & Brune, W. H. 1976, ApJ, 209, L45
Feldman, P. D., Burgh, E. B., Durrance, S. T., & Davidsen, A. F. 2000, ApJ, 538, 395
Fleming, B. T., France, K., Lupu, R. E., & McCandliss, S. R. 2010, ApJ, 725, 159
Fogel, J. K. J., Bethell, T. J., Bergin, E. A., Calvet, N., & Semenov, D. 2011, ApJ, 726, 29
France, K., Andersson, B.-G., McCandliss, S. R., & Feldman, P. D. 2005, ApJ, 628, 750
France, K., Linsky, J. L., Brown, A., Froning, C. S., & Béland, S. 2010, ApJ, 715, 596
France, K., McCandliss, S. R., & Lupu, R. E. 2007, ApJ, 655, 920
France, K., Yang, H., & Linsky, J. 2011, ApJ, 729, 7
George, T., Urban, W., & Lefloch, A. 1994, J. Mol. Spectrosc., 165, 500
Goldberg, L., Parkinson, W. H., & Reeves, E. M. 1965, ApJ, 141, 1293
Gorti, U., & Hollenbach, D. 2002, ApJ, 573, 215
Gorti, U., & Hollenbach, D. 2009, ApJ, 690, 1539
Günther, H. M., Liefke, C., Schmitt, J. H. M. M., Robrade, J., & Ness, J. 2006, A&A, 459, L29
Günther, H. M., & Schmitt, J. H. M. M. 2008, A&A, 481, 735
Habart, E., Boulanger, F., Verstraete, L., Walmsley, C. M., & Pineau des Forêts, G. 2004, A&A, 414, 531
Habing, H. J. 1968, Bull. Astron. Inst. Netherlands, 19, 421
Hartigan, P., Edwards, S., & Pierson, R. 2004, ApJ, 609, 261
Herczeg, G. J., Linsky, J. L., Valenti, J. A., Johns-Krull, C. M., & Wood, B. E. 2002, ApJ, 572, 310
Herczeg, G. J., Linsky, J. L., Walter, F. M., Gahm, G. F., & Johns-Krull, C. M. 2006, ApJS, 165, 256
Herczeg, G. J., Wood, B. E., Linsky, J. L., Valenti, J. A., & Johns-Krull, C. M. 2004, ApJ, 607, 369
Hinkle, K., Wallace, L., Valenti, J., & Ayres, T. 2005, in Ultraviolet Atlas of the Arcturus Spectrum, 1150–3800 Å, ed. K. Hinkle, L. Wallace, J. Valenti, & T. Ayres (San Francisco, CA: ASP)
Hubert, B., Gérard, J. C., Gustin, J., Shematovich, V. I., Bisikalo, D. V., Stewart, A. I., & Gladstone, G. R. 2010, Icarus, 207, 549
Ingleby, L., et al. 2009, ApJ, 703, L137
Ingleby, L., et al. 2011, ApJ, submitted
Jayawardhana, R., Coffey, J., Scholz, A., Brandeker, A., & van Kerkwijk, M. H. 2006, ApJ, 648, 1206
Jensen, E. L. N., & Mathieu, R. D. 1997, AJ, 114, 301
Johns-Krull, C. M., Valenti, J. A., & Linsky, J. L. 2000, ApJ, 539, 815
Kastner, J. H., Zuckerman, B., Hily-Blant, P., & Forveille, T. 2008, A&A, 492, 469
Kenyon, S. J., & Hartmann, L. 1995, ApJS, 101, 117
Krasnopolsky, V. A., & Feldman, P. D. 2002, Icarus, 160, 86
Kraus, A. L., & Hillenbrand, L. A. 2009, ApJ, 704, 531
Kurucz, R. L. 1993, kurucz.harvard.edu
Lahuis, F., van Dishoeck, E. F., Blake, G. A., Evans, N. J., II, Kessler-Silacci, J. E., & Pontoppidan, K. M. 2007, ApJ, 665, 492
Lawson, W. A., Lyo, A., & Muzerolle, J. 2004, MNRAS, 351, L39
Lecavelier des Etangs, A., et al. 2001, Nature, 412, 706
Le Floch, A. C., Launay, F., Rostas, J., Field, R. W., Brown, C. M., & Yoshino, K. 1987, J. Mol. Spectrosc., 121, 337
Liszt, H. S., Pety, J., & Lucas, R. 2010, A&A, 518, A45
Luhman, K. L., & Steeghs, D. 2004, ApJ, 609, 917
Lupu, R. E., Feldman, P. D., Weaver, H. A., & Tozzi, G. 2007, ApJ, 670, 1473
Mamajek, E. E., Lawson, W. A., & Feigelson, E. D. 1999, ApJ, 516, L77
Mandy, M. E., & Martin, P. G. 1993, ApJS, 86, 199
Mathis, J. S. 1990, ARA&A, 28, 37
McPhate, J. B., Feldman, P. D., McCandliss, S. R., & Burgh, E. B. 1999, ApJ, 521, 920
Morton, D. C., & Noreau, L. 1994, ApJS, 95, 301
Muzerolle, J., Calvet, N., & Hartmann, L. 2001, ApJ, 550, 944
Najita, J., Carr, J. S., Glassgold, A. E., Shu, F. H., & Tokunaga, A. T. 1996, ApJ, 462, 919
Najita, J. R., Carr, J. S., Glassgold, A. E., & Valenti, J. A. 2007, in Protostars and Planets V, ed. B. Reipurth, D. Jewitt, & K. Keil (Tucson, AZ: Univ. Arizona Press), 507
Najita, J., Carr, J. S., & Mathieu, R. D. 2003, ApJ, 589, 931
Osterman, S., et al. 2010, arXiv:1012.5827O
Pascucci, I., et al. 2006, ApJ, 651, 1177
Qi, C., et al. 2004, ApJ, 616, L11
Quast, G. R., Torres, C. A. O., de La Reza, R., da Silva, L., & Mayor, M. 2000, in IAU Symp. 200, Birth and Evolution of Binary Stars, ed. B. Reipurth & H. Zinnecker (Cambridge: Cambridge Univ. Press), 28
Ramsay Howat, S. K., & Greaves, J. S. 2007, MNRAS, 379, 1658
Roberge, A., Feldman, P. D., Lagrange, A. M., Vidal-Madjar, A., Ferlet, R., Jolly, A., Lemaire, J. L., & Rostas, F. 2000, ApJ, 538, 904
Roberge, A., et al. 2001, ApJ, 551, L97
Rodriguez, D. R., Kastner, J. H., Wilner, D., & Qi, C. 2010, ApJ, 720, 1684
Salyk, C., Blake, G. A., Boogert, A. C. A., & Brown, J. M. 2007, ApJ, 655, L105
Salyk, C., Pontoppidan, K. M., Blake, G. A., Lahuis, F., van Dishoeck, E. F., & Evans, N. J., II. 2008, ApJ, 676, L49

Saucedo, J., Calvet, N., Hartmann, L., & Raymond, J. 2003, ApJ, 591, 275
Sheffer, Y., Rogers, M., Federman, S. R., Abel, N. P., Gredel, R., Lambert, D. L., & Shaw, G. 2008, ApJ, 687, 1075
Shull, J. M., France, K., Danforth, C. W., Smith, B., & Tumlinson, J. 2010, ApJ, 722, 1312
Sicilia-Aguilar, A., et al. 2009, ApJ, 701, 1188
Sitko, M. L., Bernstein, L. S., & Glinski, R. J. 2008, ApJ, 680, 1426
Sonnentrucker, P., Welty, D. E., Thorburn, J. A., & York, D. G. 2007, ApJS, 168, 58
Stecher, T. P., & Williams, D. A. 1967, ApJ, 149, L29
Stempels, H. C., & Gahm, G. F. 2004, A&A, 421, 1159
Torres, C. A. O., Quast, G. R., da Silva, L., de La Reza, R., Melo, C. H. F., & Sterzik, M. 2006, A&A, 460, 695
van Dishoeck, E. F., & Black, J. H. 1988, ApJ, 334, 771
Vasyunin, A. I., Wiebe, D. S., Birnstiel, T., Zhukovska, S., Henning, T., & Dullemond, C. P. 2011, ApJ, 727, 76
Vidal-Madjar, A., et al. 1994, A&A, 290, 245
Walter, F. M., et al. 2003, AJ, 126, 3076
White, R. J., & Ghez, A. M. 2001, ApJ, 556, 265
Yang, H., Linsky, J., & France, K. 2011, ApJ, 730, L10